Available online at www.sciencedirect.com
ScienceDirect
Journal of Catalysis 246 (2007) 266–276
JOURNAL OF CATALYSIS
www.elsevier.com/locate/jcat

NMR spectroscopic and theoretical evidence of cinchona alkaloid–ketopantolactone complex formation in aprotic solvents: Implications for the mechanism of Pt-catalyzed enantioselective hydrogenation of activated ketones

Tamás A. Martinek [a], Tibor Varga [b], Ferenc Fülöp [a], Mihály Bartók [b,c,*]

[a] *Institute of Pharmaceutical Chemistry, University of Szeged, Eötvös u 6, H-6720 Szeged, Hungary*
[b] *Department of Organic Chemistry, University of Szeged, Dóm tér 8, H-6720 Szeged, Hungary*
[c] *Organic Catalysis and Stereochemistry Research Group of the Hungarian Academy of Sciences, Dóm tér 8, H-6720 Szeged, Hungary*

Received 16 October 2006; revised 27 November 2006; accepted 27 November 2006

Available online 17 January 2007

Abstract

NMR spectroscopy (standard 2D NMR spectroscopic methods and diffusion-ordered NMR spectroscopy) and theoretical calculations (ab initio modeling at the density functional level and natural bond orbital analysis) were used to verify formation of supramolecular complexes between the pairs O-methylcinchonine–ketopantolactone (KPL) and β-isocinchonine–KPL in deuterobenzene solution. The first direct evidence was found on the interaction of the lone pair of the quinuclidine N atom and the prochiral keto-carbonyl group of the KPL. Strong $n_N \rightarrow \pi^*$ interactions were observed between the nonbonding orbital of the quinuclidine N atom and the π^* antibonding orbitals of the C=O bonds. The complex was demonstrated experimentally to be stabilized not only by the H bonds between H5′ of the chiral modifier and the KPL, but also, depending on the structure of the cinchona alkaloid, by those between H8 and H9 and the KPL. In aprotic solvents, this type of experimentally verified adduct may be present on the Pt surface and participate in chiral induction in the Orito reaction.

Keywords: Enantioselective hydrogenation; Chiral induction; Supramolecular complex; Intermediate complex; Cinchona; Ketopantolactone; NMR; Molecular modeling

1. Introduction

The synthesis of optically active compounds is an important field of organic chemical research [1–5]. Enantioselective heterogeneous catalytic hydrogenation exhibits a number of advantages for the preparation of chiral compounds. Probably the best-characterized such reaction is the hydrogenation of α-ketoesters—the Orito reaction [6,7] (Scheme 1)—in which enantioselectivities exceeding 96–98% have been attained [8–11]. The catalyst in the Orito reaction is Pt modified by cinchona alkaloids.

The main objectives of recent studies on the Orito reaction have been to expand its field of utilization, to elucidate the reaction mechanism, and to interpret chiral induction in this context. The results published in this field have been reviewed regularly [12–17]. It is generally accepted that the intermediate responsible for enantioselection is the 1:1 complex of the cinchona alkaloid as chiral modifier and the substrate [18,19]. No consensus has been reached, however, concerning the structure of this intermediate. The main types possibilities are presented schematically in Scheme 2. Besides computational methods, experimental approaches have been applied to verify the structures of the 1:1 intermediates of pyruvates or ketopantolactone (KPL) and cinchonidine [31–33]. ESI-MS/MS measurements [31] and in situ ATR-IR spectroscopy [32,33] studies indicate H bonding between the protonated quinuclidine moiety in an anti-open (open-3) conformation of

* Corresponding author. Fax: +36 62 544 200.
E-mail address: bartok@chem.u-szeged.hu (M. Bartók).

0021-9517/$ – see front matter
doi:10.1016/j.jcat.2006.11.033

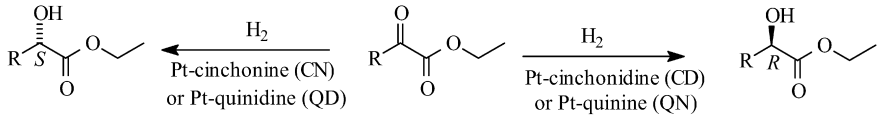

R = Me (ethyl pyruvate = EP), R = Ph (ethyl benzoylformate = EBF)

Scheme 1. Orito reaction.

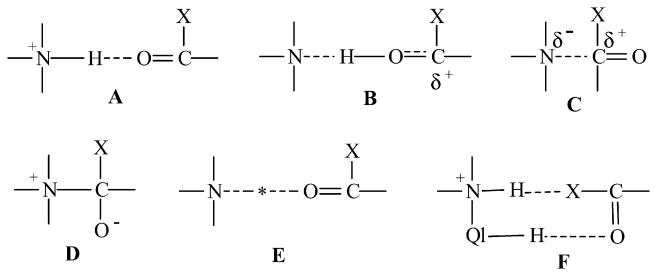

Scheme 2. Proposed intermediates in the Orito reaction: **A** [18,19], **B** [19,20], **C** [21–23], **D** [24], **E** [25–27]], **F** [28–30] (X = activating group, Ql = quinolinyl).

cinchonidine and the substrate. Under ultrahigh vacuum conditions in the case of 1-(1-naphthyl)ethylamine and methyl pyruvate, the presence of the 1:1 docking complex was recently proven by means of RAIRS spectral [34,35] and STM studies [36]. A complex of zwitterion type also has been proposed [24] (Scheme 2, **D**), but the existence of such zwitterions is a matter of dispute [37]. Efforts aimed at the experimental verification of the structure of the intermediate have been reported [24,28,29,31–36]; however, these efforts—except for ATR-IR measurements [32,33]—were performed under experimental conditions vastly different from those of the Orito reaction.

Our present goal was to investigate a minimal system in which the active H of C9–OH in cinchonine (CN) is removed. The model systems chosen were the pairs O-methylcinchonine (MeOCN)–KPL and β-isocinchonine (β-ICN)–KPL in deuterobenzene (C_6D_6) solution (Scheme 3). In these systems, only functional groups essential for the Pt surface-catalyzed hydrogenation and the enantiodifferentiation are present, without other chemical features potentially leading to "noise." Regarding the substrate, a further advantage is the rigidity of the lactone ring, which simplifies modeling. NMR spectroscopy and molecular modeling were used to examine the proposed substrate–modifier complex in solution and to determine its structural features. In the hydrogenation of KPL, the formation of excess (*S*)-PL was observed in the presence of cinchonine in toluene, whereas over Pt β-ICN as chiral catalyst, the major enantiomer was (*R*)-PL [30]. Thus, unexpected enantioselectivity inversion occurred, despite the fact that the configurations of C8 and C9 (responsible for the enantioselection) were the same.

NMR spectroscopy [37–44] and molecular modeling (to refer only to papers published since 2003 [33,44–55]) have already yielded a large amount of information contributing to a better knowledge of the mechanism of the Orito reaction. The manuscript describe new NMR spectroscopic and computational study indicating a supramolecular complex in apolar solution of type **C** ↔ **D** (Scheme 2), which might play roles in the enantioselective hydrogenation of activated ketones.

2. Experimental

2.1. Materials

C_6D_6 (99.5 at% D) purchased from Acros was distilled from $LiAlH_4$ under an argon atmosphere before use to eliminate traces of water. KPL (dihydro-4,4-dimethyl-2,3-furandione, 97%, Aldrich) was subjected to azeotropic distillation with toluene to remove water. Before use, the crystals were dried over KOH in vacuum at 363 K for 24 h. MeOCN was made by a known procedure [56]. β-ICN preparation has been described elsewhere [57]. MeOCN and β-ICN were dried over KOH in vacuum at 363 K for 24 h.

Engelhard E4759 (E4759) 5% Pt/Al_2O_3 was pretreated in a fixed-bed reactor by flushing with 30 mL min^{-1} He at 300–673 K for 30 min and 30 mL min^{-1} H_2 at 673 K for 100 min. After cooling to room temperature in H_2, the catalyst was flushed with He for 30 min and was stored until use.

2.2. Hydrogenation

The hydrogenation procedure and analysis were performed as described previously [30] under standard conditions: 12.5 mg E4759, 2 mL toluene, [modifier] = 0.01 mM L^{-1}, 295–298 K, 1 bar H_2, 0.5 mM KPL, 800–900 rpm. For cinchonine, MeOCN and β-ICN, the ee's were 56% (*S*), 2% (*S*), and 48% (*R*), respectively.

2.3. ESI-MS measurements

The ESI-MSD ion-trap (Agilent 1100 LC-MSD trap SL ion-trap MS) was operated in positive ion mode as described earlier [30]. Solvent: MeOH/0.1% AcOH; flow rate: 0.5 mL min^{-1}; concentration of sample: 0.1 μM L^{-1}; injected volume 1.5 μL.

2.4. NMR experiments

Indicated amounts of KPL and MeOCN or β-ICN were added to 500 μL C_6D_6. After solvation (2–3 min), the solution was transferred to a 5-mm NMR tube. NMR measurements were performed on a Bruker *Avance* DRX 400 MHz spectrometer with a multinuclear probe with a *z*-gradient coil in C_6D_6 solution at 303.1 K. For NOESY, 400 and 600 ms mixing

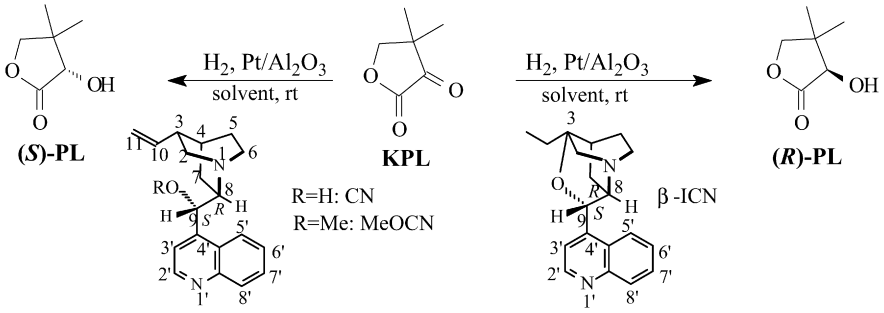

Scheme 3. The Orito reaction of KPL (PL = pantolactone).

times were used; the number of scans was 64. The TOCSY measurements were performed with homonuclear Hartman–Hahn transfer with the MLEV17 sequence, with an 80 ms mixing time; the number of scans was 32. For all the 2D spectra, 2k time domain points and 512 increments were applied. The processing was carried out using a cosine-bell window function, single zero filling, and automatic baseline correction.

The pulsed-field gradient spin-echo (PFGSE) NMR measurements were performed with the stimulated echo and longitudinal eddy current delay (LED) sequence [58]; 2 ms was used for the dephasing/refocusing gradient pulse length (δ), and 100 ms for the diffusion delay (Δ). The gradient strength was changed quadratically from 5 to 95% of the maximum value (B-AFPA 10 A gradient amplifier) and the number of steps was 16. Each measurement was run with 32 scans and 16k time domain points. For the processing, an exponential window function and single zero filling were applied. During the diffusion measurements, the temperature fluctuation was <0.1 K. Before the diffusion NMR scans, all the samples were equilibrated for 30 min. For the data analysis, the fitted points were truncated to 12, because the low concentration and the large differences in the diffusion coefficients caused fluctuations of the disappearing integrated intensities of TMS in the high-field gradient region.

2.5. Molecular modeling

Molecular modeling was carried out on an HP xw6000 workstation and an SGI Altix 3000. The Chemical Computing Group's Molecular Operating Environment was used for the force field calculations (MMFF94) [59] and input generation. In ab initio quantum chemical calculations, the molecular structure, stereochemistry, and geometry were exclusively defined in terms of their z-matrix internal coordinate system. The optimizations and the NMR shielding tensor calculations were achieved with the Gaussian 03 program [60]. The optimizations were performed in a cascade manner: force field—HF/3-21G—B3LYP/6-31G*. The NMR shifts were calculated by using the GIAO method [61] at the HF/6-31G* level. All other parameters were set as default in Gaussian 03. The natural bond orbital (NBO) analysis was performed with the NBO 5.0 code implemented in Gaussian 03.

3. Results and discussion

3.1. NMR measurements

The ^{1}H-NMR spectra of the mixture of the model cinchona alkaloids (0.8 mmol L^{-1}) and KPL (72 mmol L^{-1}) revealed line broadening for several characteristic proton signals of the cinchonas, accompanied by marked chemical shift changes (Fig. 1). The drifts of the chemical shifts were time-dependent, reaching their final values in 1 h. Concomitantly, new sets of KPL signals appeared besides the original KPL resonances assigned to the pure compound (CH_2 at 3.35 ppm and 2 CH_3 at 0.57 ppm). For the CH_2 protons of KPL mixed with MeOCN, a singlet was observed at 4.01 ppm, which underwent chemical exchange (Fig. 1 and Fig. S1 in the supporting information) with two pairs of scalarly coupled doublets at 4.90, 3.78 and 4.97, 3.78 (J = 10.1 Hz). The corresponding signals for KPL mixed with β-ICN were detected at 4.05 (singlet), 4.77, 3.88 (doublets), and 4.81, 386 (doublets). All of the new KPL signals appeared within 10 min after mixing at the concentrations generally applied during the Orito reaction. Interestingly, the new singlet KPL exhibited a slower increase, whereas the doublets remained almost constant from the first measurement point. To double-check the origin of the resonances in question, concentration-dependent measurements were carried out as well (Fig. 2). The results show that the signal intensities correlate with the KPL concentration.

Chemical exchange cross-peaks could not be observed between the new KPL species and the residual pure compound, but these CH_2 resonances could be readily assigned using the HMBC connectivity patterns and their NOE interactions to the CH_3 signals at around 1.56 ppm. The time dependence of the integrated intensities of the new KPL peaks exhibited good correlation with the extent of the chemical shift changes observed for the cinchona modifiers (Figs. 1 and 2).

The final chemical shift changes in the equilibrated mixtures relative to the pure cinchona samples are given in Fig. 3. For MeOCN, the highest downfield shift (^{1}H-$\Delta\delta$ = 1.02 ppm) was detected for H9 and the highest upfield shift (^{1}H-$\Delta\delta$ = −0.95 ppm) related to H7eq. β-ICN exhibited the highest downfield shift (^{1}H-$\Delta\delta$ = 0.64 ppm) for H5′; the highest upfield shift, for H6ax (^{1}H-$\Delta\delta$ = −0.41 ppm). The higher substrate concentration had no significant effect on the chemical shifts in the equilibrated samples, whereas the rate of the chemical shift drift was dependent on the concentration. It should be

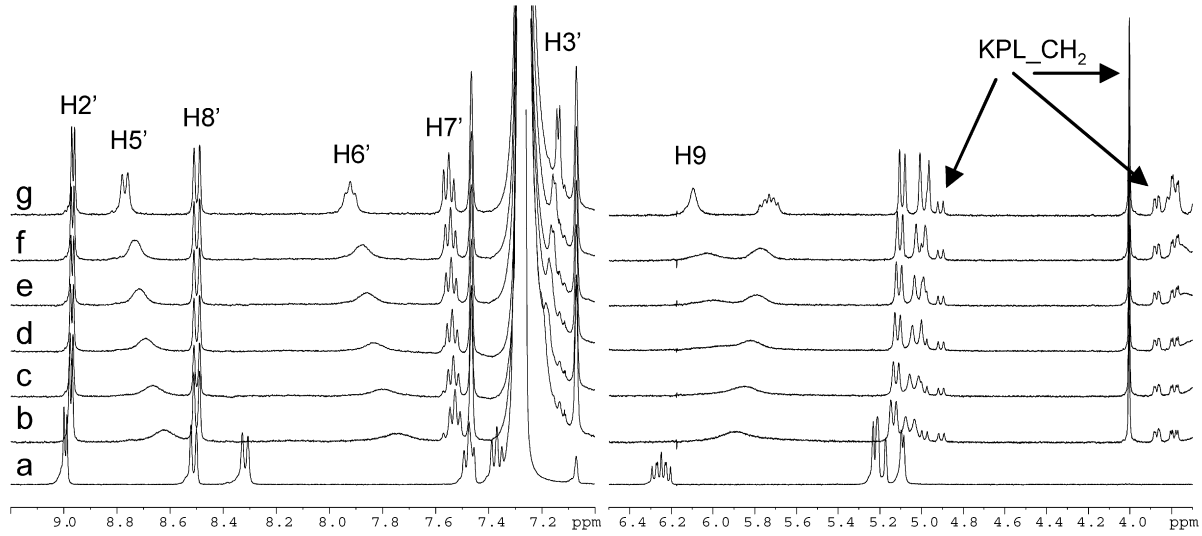

Fig. 1. Time-dependent chemical shift drifts of certain MeOCN signals and the appearance of the new sets of KPL signals upon mixing MeOCN (0.8 mmol L^{-1}) and KPL (72 mmol L^{-1}) in C_6D_6 (for abbreviations, see Scheme 3): (a) 0 (no KPL added), (b) 12, (c) 24, (d) 36, (e) 48, (f) 104, and (g) 144 min.

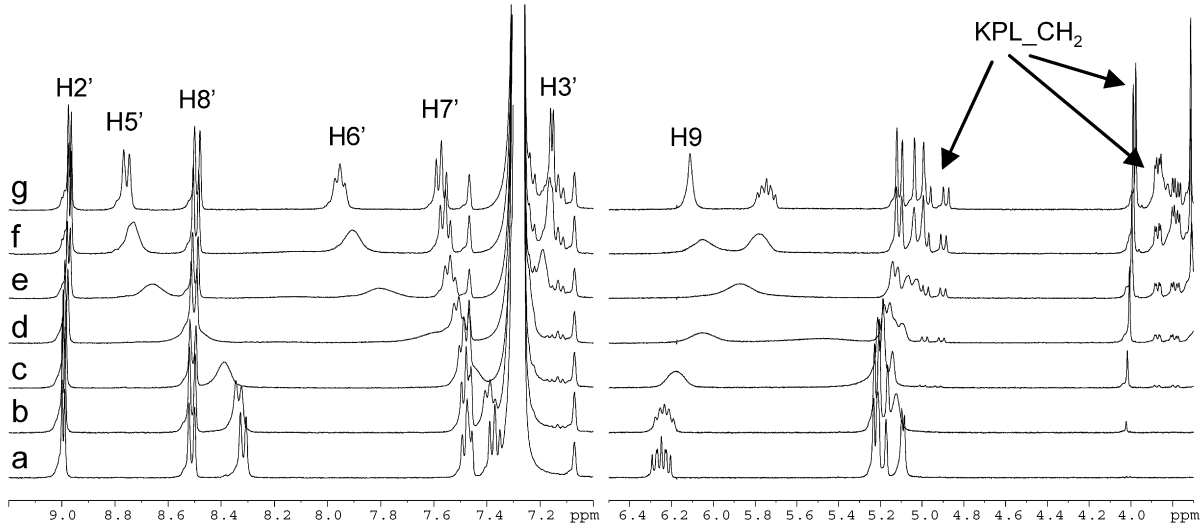

Fig. 2. Concentration-dependent chemical shift changes of certain MeOCN signals and the appearance of the new sets of KPL signals upon adding increasing amount of KPL to MeOCN (5 mmol L^{-1}) in C_6D_6 (for abbreviations, see Scheme 3): (a) 0, (b) 12, (c) 36, (d) 72, (e) 108, (f) 144, and (g) 216 mmol L^{-1}.

noted that the integrated intensity ratio of the new KPL CH_2 singlets and any of 1H intensity peaks of the cinchonas did not exceed 1:1 even for highly elevated KPL concentrations. The intensity ratio of the singlet and each of the split CH_2 signals was estimated as 0.75:0.25. For the pure KPL and cinchona samples, no changes in the spectral parameters were detected. Interestingly, the modifier-substrate complex was still observable after the sample was treated with 10 equivalent of acetic acid relative to the modifier indicating that the nucleophilic interaction can compete with an agent more acidic than H_2 adsorbed on the Pt surface [62].

These observations point to the presence of three new KPL species in interaction with the cinchona modifiers in solution. Mass spectrometry was done to rule out any cinchona-catalyzed conversion of KPL. The mass spectra recorded on the equilibrated samples by using the GC-MS and the ESI-MS techniques furnished the molecular ions of the cinchona and KPL only, with no other reaction product observed in the sample. These results strongly suggest that the marked changes in the NMR spectral parameters are due to contact interactions between the cinchonas and the KPL, and these supramolecular complexes are stabilized by weaker nonbonding interactions. From the multiplicity and the strong downfield shifts of the KPL signals, we may conclude that the bound KPL species giving rise to the CH_2 singlet are in a quasi-symmetric environment in which the benzene cannot exert its solvent shielding directly. The two split-doublet pairs belonging to KPL moieties are indicative of a magnetically asymmetric environment, where the solvent shielding presumably still occurs on one side of the KPL ring.

To test the association in the solution phase, diffusion-ordered NMR spectroscopy was carried out on both the pure compounds and the mixtures. A stimulated gradient echo and LED were used for the diffusion NMR measurements [58].

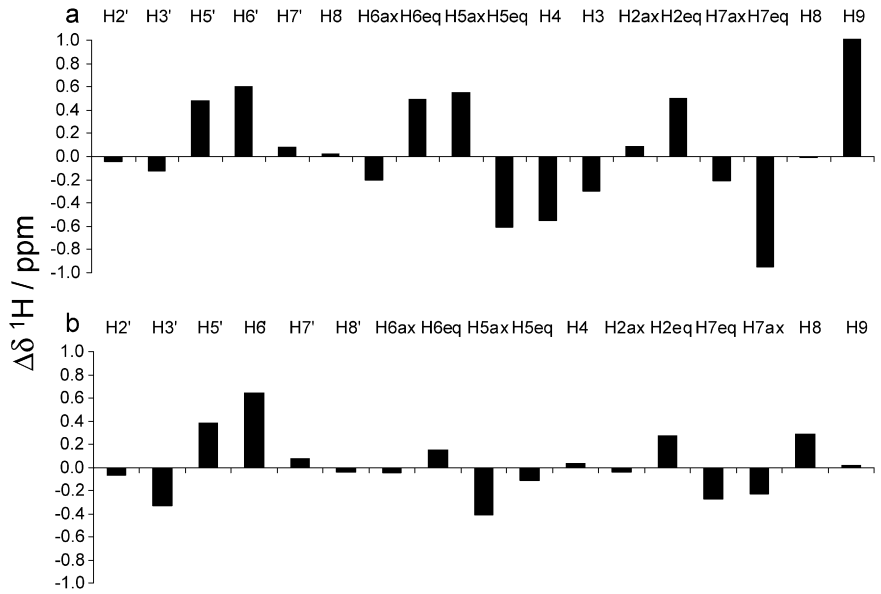

Fig. 3. Chemical shift changes for indicator protons observed in equilibrated samples (after 120 min) for MeOCN (a) and β-ICN (b) (for abbreviations, see Scheme 3).

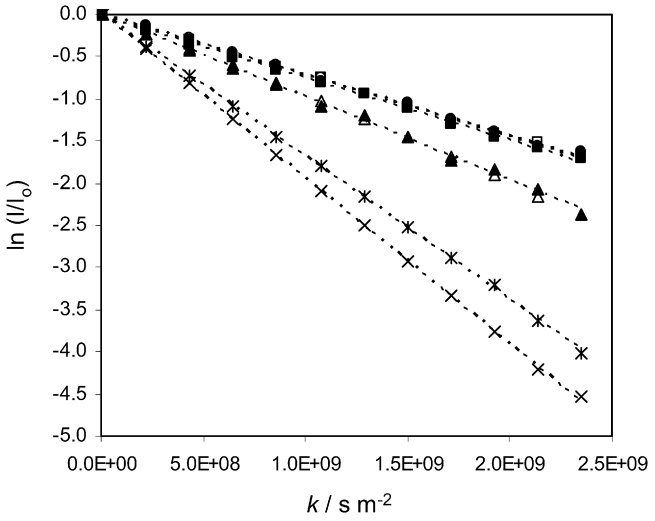

Fig. 4. PFGSE decay curves: (×) for TMS, (∗) for pure KPL at 3.35 ppm, (▲) for pure MeOCN at 9.00 ppm, (■) for the KPL–MeOCN mixture at 4.01 ppm, and (●) for the KPL–MeOCN mixture at 8.96 ppm; (△) for pure β-ICN at 9.04 ppm, (□) for the KPL–β-ICN mixture at 4.05 ppm, and (○) for the KPL–β-ICN mixture at 8.97 ppm.

TMS was applied as an internal size reference. Because the molecular volumes of TMS and KPL are comparable to that of the solvent benzene molecule, the apparent hydrodynamic radius (r) were estimated from the diffusion coefficient (D) using the Sutherland–Einstein equation, with the Stokes–Einstein equation applied for the larger species (cinchonas and complexes) [63,64]. The details of the calculation are given in the supporting information. The PFGSE decay curves furnished good-quality data for determining the diffusion coefficients and estimating the apparent hydrodynamic radii (Fig. 4 and Table 1).

The experimental radii for the pure cinchonas are in good agreement with the theoretical values (5.43 Å for MeOCN and 5.50 Å for β-ICN), indicating that the method is sufficiently robust. The radius obtained for KPL is relatively overestimated compared with the theoretical value for the isolated molecule, suggesting effective solvation by the benzene. The measurements clearly reveal that the radii measured in the mixtures both at the characteristic H2′ cinchona signals (at around 9.96 ppm) and at the CH_2 singlets of the newly appeared KPL species (4.01 ppm) are similar and significantly greater than those of the pure samples. For the split CH_2 doublets, the measurements could be carried out accurately only on the β-ICN + KPL sample; in the MeOCN + KPL sample, these signals overlap with the olefinic protons. Nevertheless, the diffusion coefficients are practically identical to those obtained for the CH_2 singlets. This is explained by the chemical exchange leading to averaging, which is sufficiently fast on the NMR relaxation time scale. These findings prove the presence of cinchona–KPL supramolecular complexes in benzene solution. We emphasize that the measured radius for the proposed substrate–modifier adduct considerably exceeds the values calculated for the 1:1 cinchona:KPL complexes displayed in Fig. 5 (r = 5.99 Å for

Table 1
The apparent hydrodynamic radii estimated by diffusion NMR

Sample	Peak (ppm)	D ($\times 10^{-9}$ m^2 s^{-1})	R^{2b}	Radius (Å)
TMS	0.00	1.960	0.9998	3.96[a]
Pure KPL	3.35	1.696	0.9998	4.57
Pure MeOCN	9.00	0.989	0.9973	5.24
MeOCN + KPL	8.96	0.717	0.9975	7.22
MeOCN + KPL	4.01	0.733	0.9988	7.07
Pure β-ICN	9.04	1.007	0.9992	5.14
β-ICN + KPL	8.97	0.739	0.9990	7.00
β-ICN + KPL	4.05	0.723	0.9988	7.16

[a] Reference value taken from the estimation of the solute cavity radius by using the keyword VOLUME in Gaussian 03.
[b] Regression coefficients of linear fits in Fig. 3.

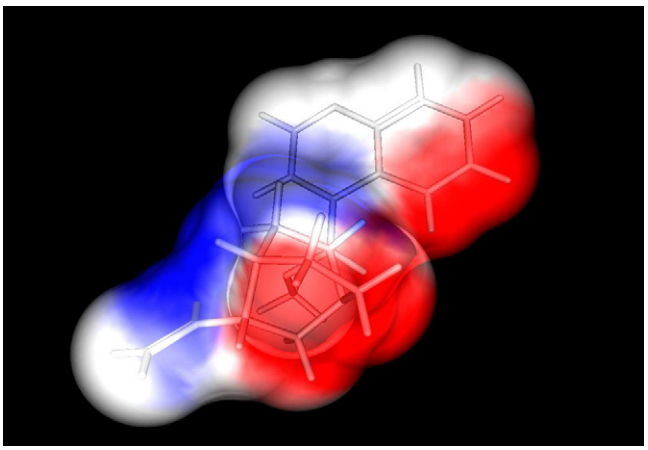

Fig. 5. ^{1}H-NMR chemical shift changes projected onto the Connolly surface of MeOCN in its most stable open-3 conformation (^{1}H-$\Delta\delta > 0.4$, red; ^{1}H-$\Delta\delta < -0.4$, blue).

MeOCN and 6.05 Å for β-ICN). The anomalously increased size, the symmetric magnetic environment of the KPL CH_2 singlet, and the presence of the two additional asymmetric KPL species give rise to the possibility of the formation of a quasi-symmetric 2:1 adduct that is in chemical exchange with the asymmetric 1:1 adducts.

Following proof of the solution-phase association between the cinchonas and KPL, an attempt was made to determine the spatial arrangement of the adducts. First, the NOESY spectra were evaluated with respect to the possible conformational changes induced in the cinchonas in by the presence of KPL. The NOE interactions clearly showed that the pure modifiers exist predominately in their open-3 conformation (Fig. 5). The conformation exhibited only minor changes on mixing with KPL, thereby suggesting that the complexation occurs in the open-3 conformation of the cinchonas. For MeOCN, the coupling ^{3}J(H8, H9) decreased from 4 to <1 Hz, pointing to a small dihedral shift along the C8–C9 bond from gauche toward orthogonal. Unfortunately, intermolecular NOESY cross-peaks could not be observed, which may be due to the specific geometry of the adduct and/or to their destruction by the averaging effect of the fast chemical exchange between the bound and unbound forms of the cinchonas (see the line broadening and signal coalescence in Fig. 1). Nevertheless, the information encoded in the chemical shift changes can be exploited to gain a picture of the 3D structure. The ^{1}H chemical shift differences between the MeOCN signals of the pure form and the adduct were projected onto the Connolly surface of the open-3 conformation of the modifier. This representation points to the molecular interface, which presumably plays a role in the binding of KPL. Our findings support the view that the quinuclidine N atom, H9, and the C5′ region of the quinoline ring are responsible for the cinchona–KPL interaction. Similar results were obtained for β-ICN.

3.2. Theoretical calculations

Molecular modeling was carried out at the ab initio quantum chemical level to interpret the experimental NMR spectral parameter changes. The structural hypothesis must satisfy the following requirements: (i) There must be two comparably stable asymmetric 1:1 adducts; (ii) the 1:1 complexes must be reasonably readily converted to the symmetric 2:1 adducts to facilitate the chemical exchange; and (iii) the experimental radii and chemical shift changes must correlate with the values calculated from the models. Extreme care was taken to remove any residual water from the samples; accordingly, no residual water signal was detected at 0.4 ppm. Therefore, it is unlikely that protonated reactants can arise under the conditions applied, which is a suggested prerequisite of cinchona–KPL complex formation in models **A**, **B**, and **F** in Scheme 2. Moreover, the symmetric 2:1 complex indicated by the experimental data cannot be constructed by using the protonated H-bonding models. The formation of stable intermediate **D** is not supported by the ^{13}C chemical shifts observed, which is in line with the literature results [37]. By following these principles, we constructed 1:1 and 2:1 adducts according to model **C**. The structures were optimized in a cascade manner: force field (MMFF94) [59]—HF/3-21G—B3LYP/6-31G* [60]. The resulting 1:1 adducts are labeled by the enantioselection facilitated by the geometry: ProR and ProS. For the 2:1 complexes, two possible conformations were obtained, and, depending on the relative distances between the quinuclidine N atoms and the C=O C atoms in KPL, these structures were also labeled ProR and ProS. The lowest-energy geometries are depicted in Fig. 6.

Comparing the theoretical radii of the 2:1 complexes (r = 6.90 Å for MeOCN, and r = 7.15 Å for β-ICN) with the experimental values (Table 1) indicates very good agreement, providing supportive evidence for the prevailing 2:1 adducts in solution. From the 3D structures obtained from the ab initio optimization, theoretical NMR chemical shifts were calculated for the isolated cinchona structures, and for the adducts via the GIAO methodology [61] at the HF/6-31G* level, to enable a quantitative comparison with the observed parameters. The resulting theoretical values were referenced to TMS, and the chemical shift differences between the isolated cinchonas and the complexes were compared (Table S1). The Pearson correlation coefficients (Table 2) reveal an acceptable overall agreement between the calculated and the experimental $\Delta\delta^{1}$H values, taking into account the limited accuracy of the ab initio NMR chemical shift calculations in the absence of the solvent shielding effect. Thus, the chemical shift difference patterns support the proposed models shown in Fig. 6. As a negative control, the lowest-energy geometries of the protonated 1:1 cinchona–KPL complexes were calculated according to model **A** in Scheme 2 (geometries are given in Fig. S2). The protonated complexes displayed no correlation with the experimental data.

The complexes are stabilized by electrostatic attractions between the partially positive C=O carbons of KPL and the negative charge center on the lone pair of the N atom. An additional energy gain is provided by the weak C=O–H–C H bonds [65], where the donor atoms are H9 and H5′ for MeOCN, and H8 and H5′ for β-ICN. These H atoms exhibited a high downfield shift on NMR. All three O atoms of KPL can play a role as acceptor pillars in these C=O–H–C H bonds, depending on the nature

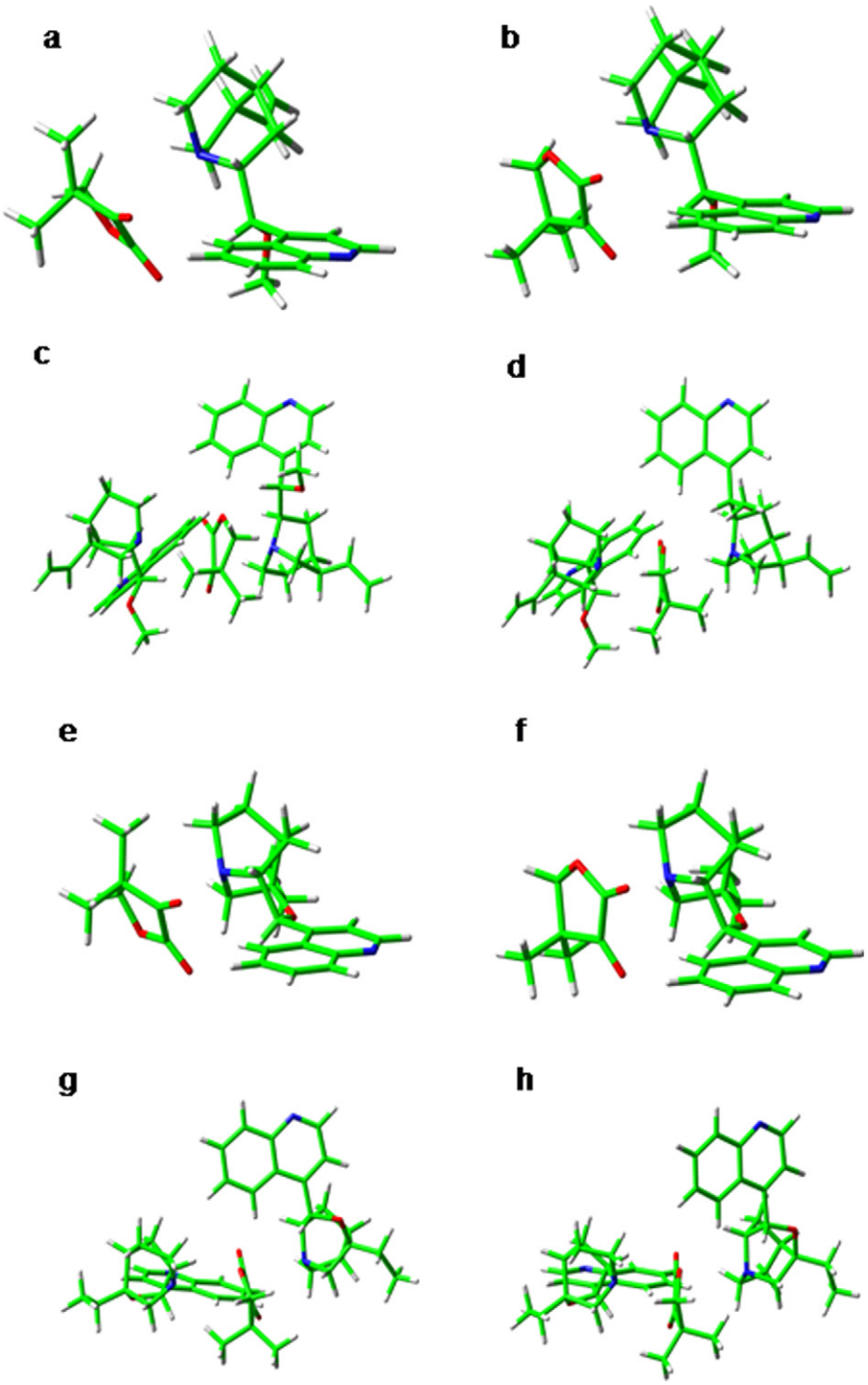

Fig. 6. Ab initio geometries (B3LYP/6-31G*) of the hypothesized substrate–modifier adducts MeOCN + KPL_1:1_ProS (a), MeOCN + KPL_1:1_ProR (b), MeOCN + KPL_2:1_ProS (c), MeOCN + KPL_2:1_ProR (d), β-ICN + KPL_1:1_ProS (e), β-ICN + KPL_1:1_ProR (f), β-ICN + KPL_2:1_ProS (g), and β-ICN + KPL_2:1_ProR (h).

Table 2
Pearson correlations between the ab initio calculated and the experimental NMR shift changes of the cinchona moieties

	1:1_ProR	1:1_ProS	2:1_ProR	2:1_ProS	Protonated complex
MeOCN + KPL	0.59	0.58	0.56	0.55	−0.06
β-ICN + KPL	0.29	0.41	0.39	0.52	−0.01

of the complex, and bifurcated H bonds also can be recognized in the structures. Interestingly, the O in the lactone ring can participate in stabilizing the H bonds with the aromatic H5′ (see 2:1 adducts). The nonbonding interactions result in overall stabilization energies in the range 6.5–7.3 kcal mol^{-1} at the B3LYP/6-31G(d) level (12.0–12.9 kcal mol^{-1} at the HF/3-21G level) for the 1:1 cinchona:KPL complexes. For the 2:1 adducts,

Table 3
Ab initio energies for the studied complexes

Structure	HF/3-21G (a.u.)	B3LYP/6-31G(d) (a.u.)
KPL	−453.9078466	−459.1193877
MeOCN	−949.7587031	−961.2626669
β-ICN	−910.9669060	−921.9750399
MeOCN_1:1_ProS	−1403.6856873	−1420.3924430
MeOCN_1:1_ProR	−1403.6868884	−1420.3935596
MeOCN_2:1_ProS	−2353.4611093	−2381.6639789
MeOCN_2:1_ProR	−2353.4618087	−2381.6641038
β-ICN_1:1_ProS	−1364.8952859	−1381.1061109
β-ICN_1:1_ProR	−1364.8952434	−1381.1058865
β-ICN_2:1_ProS	−2275.8768202	−2303.0890387
β-ICN_2:1_ProR	−2275.8783605	−2303.0891904

	Stabilization energies (kcal mol^{-1})	
MeOCN_1:1_ProS	−12.01	−6.52
MeOCN_1:1_ProR	−12.76	−7.22
MeOCN_2:1_ProS	−22.50	−12.08
MeOCN_2:1_ProR	−22.94	−12.16
β-ICN_1:1_ProS	−12.88	−7.33
β-ICN_1:1_ProR	−12.86	−7.19
β-ICN_2:1_ProS	−22.06	−12.28
β-ICN_2:1_ProR	−23.03	−12.38

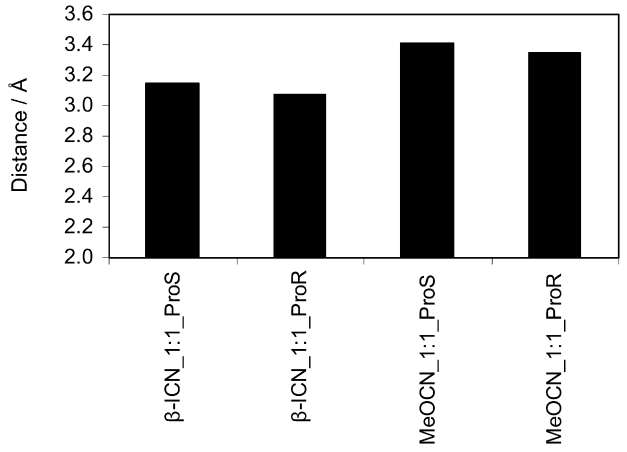

Fig. 7. Calculated N–C=O_{ketone} distances at the B3LYP/6-31G(d) level.

the stabilization energies are in the range 12.1–12.4 kcal mol^{-1} at the B3LYP/6-31G(d) level (22.1–23.0 kcal mol^{-1} at the HF/3-21G level). These values account for the association in the solution phase. The C–H···O H bonding is identified by different experimental methods too [66,67].

The significant upfield shifts measured for H7eq of MeOCN can be explained by the dihedral change along the C8–C9 bond, which orients the quinuclidine face in question above the aromatic shielding cone of the quinoline rings. This is supported by the aforementioned change in ^3J(H8, H9). Such an intense upfield shift was not observed for β-ICN, where the C8–C9 bond is rigid. The ab initio energies for the ProR and ProS complexes do not indicate significant differences (Table 3), in accordance with their experimentally observed similar concentrations in solution.

3.3. Electronic structure of the observed complexes and its possible implications for the chiral induction in the Orito reaction

Geometrical analysis of the ab initio structures reveals an important feature: The distances between the C=O C atoms and the quinuclidine N atom are well below the sum of their van der Waals radii (3.72 Å) (Fig. 7). The unusually low distances raises the question of whether there is an electron orbital overlap interaction in addition to the pure electrostatic attraction between the N and the C=O atoms. To find any electronic interaction, the conjugation effect was tested for the experimentally studied modifiers using NBO analysis. This method projects the delocalized molecular orbitals onto the combination of localized Lewis-like bonding, antibonding, nonbonding orbitals, and residual delocalization effects due to the overlaps between the localized orbitals [68]. The results clearly indicate reasonably strong $n \rightarrow \pi^*$ interactions between the nonbonding orbital of the quinuclidine N atom and the π^* antibonding orbitals of C=O bonds of the keto and the ester functional groups (Fig. 8). The stabilizing electron delocalization energies due to orbital overlaps are good indicators of the strengths of the interactions and are depicted for the n(N) $\rightarrow \pi^*$(C=O_{ketone}) orbital

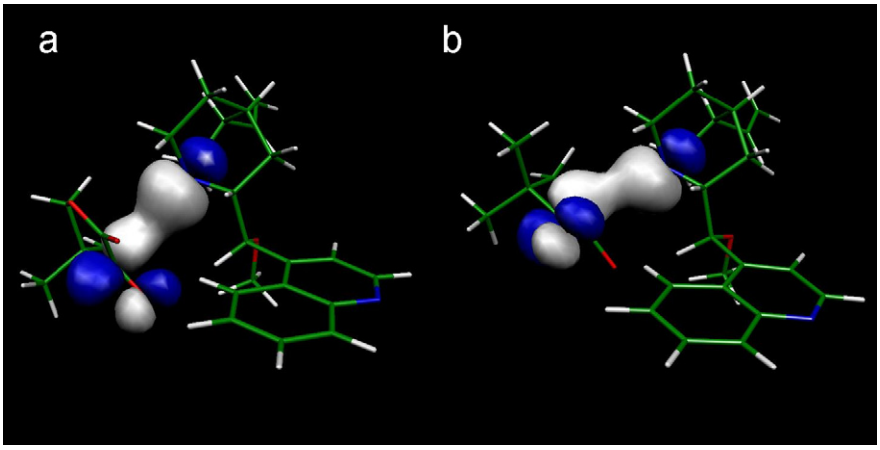

Fig. 8. $n_N \rightarrow \pi^*$(C=O_{ketone}) interactions in MeOCN + KPL_1:1_ProR (a) and MeOCN + KPL_1:1_ProS (b), revealed by the NBO calculations based on the solution phase data.

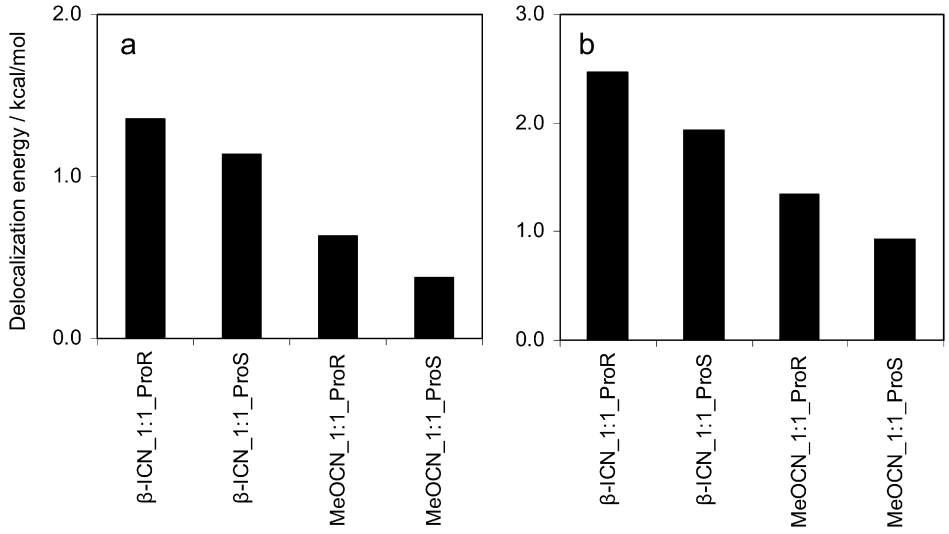

Fig. 9. Stabilizing $n_N \rightarrow \pi^*(C{=}O_{ketone})$ (a) and $n_N \rightarrow \pi^*(C{=}O_{ester})$ (b), delocalization energies obtained through a second-order perturbative analysis of the Fock matrix in the NBO basis.

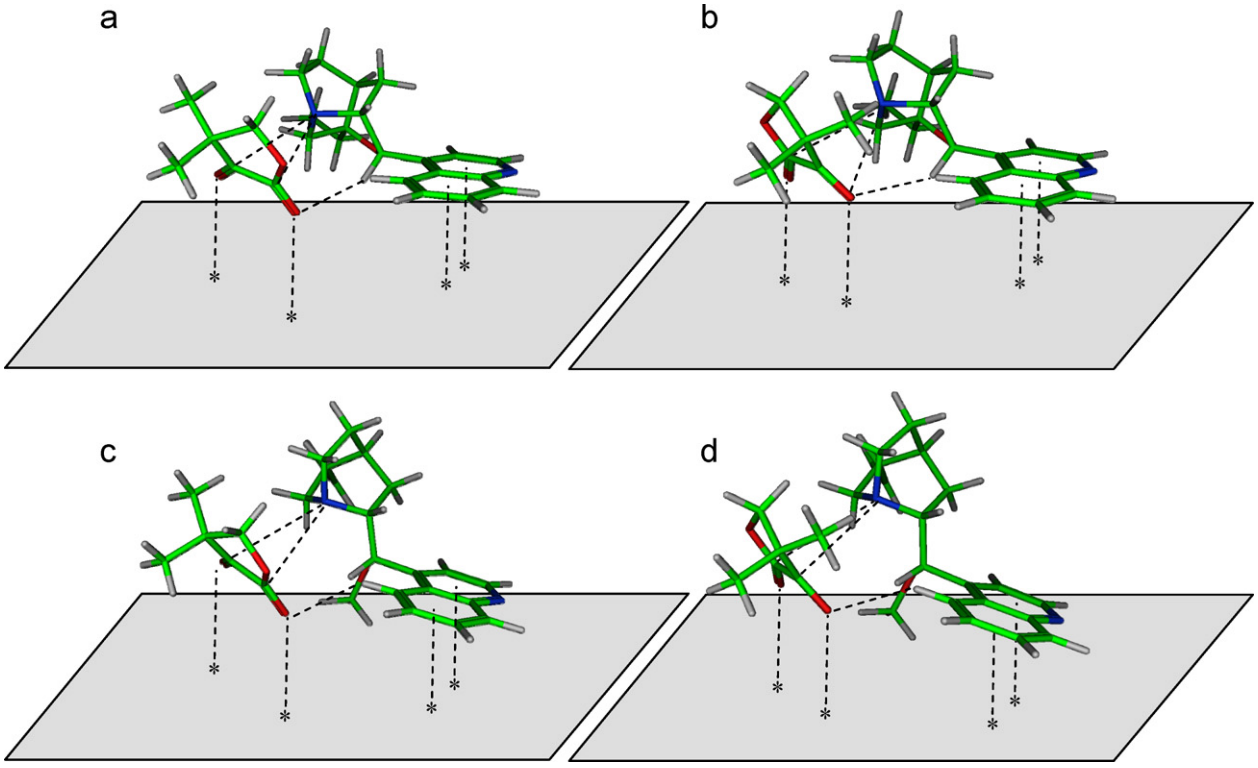

Fig. 10. The proposed structures of the adsorbed adducts for β-ICN_ProR (a), β-ICN_ProS (b), MeOCN_ProR (c), and MeOCN_ProS (d).

overlap (Fig. 9a) and for the $n(N) \rightarrow \pi^*(C{=}O_{ester})$ interaction (Fig. 9b).

Because our ab initio models correspond to the structures observed in the solution state in the absence of the Pt surface, their relevance in the Orito reaction must not be overstressed; for example, the specific positions of the C=O bonds are certainly affected by the metal surface. However, their stability, suggested by the resistance of the complexes to 10 equiv. acetic acid in solution, may allow the conclusion that the presence of such complexes over the Pt surface cannot be totally ruled out. Considering the accumulated experimental results in the literature [32–36,69,70], the N-protonated intermediate complexes cannot be ruled out either. In our opinion, the two types of intermediate complexes might compete over the surface, and their relative importance is determined by the specific conditions especially the acidity and polarity of the solvent. Experimental results on the enantioselectivity inversion upon solvent change support this approach [23].

To determine the specific geometry and electronic structures of the recently proposed nucleophilic complexes over the

Pt surface [30,71,72], accurate modeling in the presence of a Pt cluster is needed. However, preliminary models of the assumed nucleophilic intermediate complexes clearly reveal that the geometrical arrangement of the experimentally proven anchor points (quinuclidine N, and H5′) can position the substrate so that it can advantageously bind to the Pt surface as well (Fig. 10).

4. Conclusion

The most widely discussed and generally accepted models [12–17] for the mechanism of enantioselective hydrogenation of activated ketones are based on the formation of 1:1 complexes between the cinchona modifiers and the prochiral ketocarbonyl function of the substrate [18,19]. Consensus has been reached in the literature that H-bonding interactions may play important role in the structure of the intermediate complex responsible for enantioselection [28,29,32–36,48]. Under the conditions of electrophilic catalysis, the one-point or two-point H-bonding models involving protonated quinuclidine nitrogen have been proposed based on experimental evidences. It has been proposed that the nitrogen could be protonated by the H_2 adsorbed on the Pt-surface [69,70]. The exact mechanism of activation of the C=O bond decreasing the activation energy of hydrogenation, however, still remains elusive. Another open question is the stabilization of the intermediate complex under the conditions of nucleophilic catalysis (in an aprotic solvent without residual water adsorbed on the surface).

When cinchona alkaloid derivatives (MeOCN and β-ICN) and KPL were mixed in dry benzene solution, time-dependent chemical shift changes for the cinchonas and new signals for KPL bound to the modifier were detected. The spatial pattern of the chemical shift differences and the conformations of the modifiers determined by NOESY clearly demonstrated that the substrate binding occurs at the quinuclidine N atom, H9, and the quinoline H5′ region for MeOCN. The corresponding hydrogens for β-ICN are H8 and H5′. Diffusion NMR experiments corroborated the association hypothesis by revealing the co-diffusion of the cinchonas and KPL in a complex. The experimentally estimated apparent hydrodynamic radii for the adducts unequivocally showed that not only 1:1, but also 2:1 cinchona–KPL complexes must be taken into account. The modifier–substrate complex proved to be stable against significant excess of acetic acid, indicating that the nucleophilic interaction can compete with an agent more acidic than H_2 adsorbed on the Pt surface [62].

Ab initio modeling based on the experimental data predicted that the substrate–modifier adducts are stabilized at three points by (i) attraction between the partially positive C=O C atom and the negatively charged quinuclidine N atom, (ii) weak C=O···HC H bonding to the H5′ region of the quinoline moiety in various patterns, depending on the specific complex geometry, and (iii) C=O···HC H bonding to H9 (MeOCN) or H8 (β-ICN).

The NBO analysis carried out on complexes of MeOCN and β-ICN obtained by ab initio calculations unambiguously revealed that electron delocalization occurs between the quinuclidine N atom lone pair and the antibonding π^* orbitals of the C=O groups. This stabilization effect can contribute to the enantioselection step in the course of the Pt-catalyzed hydrogenation. The immediate objects of the planned research work in this field are the accurate modeling in the presence of Pt cluster and the performance of similar investigations in protic solvents, that is, under the circumstances of electrophilic catalysis.

Acknowledgments

Computational resources were provided by the High-Performance Computing Center, University of Szeged. Financial support was provided by the Hungarian National Science Foundation (OTKA grants TS044690 and T048764). T.A.M. acknowledges the award of a János Bolyai scholarship from the Hungarian Academy of Sciences.

Supporting information

^{1}H-NMR chemical shift signal assignments and ab initio calculated chemical shifts; NOESY/EXSY spectra for MeOCN + KPL and β-ICN + KPL samples; lowest-energy ab initio structures for the protonated cinchona–KPL complexes; a detailed description of the diffusion NMR methodology. Further ab initio computational data are from the authors on request.

Please visit DOI: 10.1016/j.jcat.2006.11.033.

References

[1] H. Brunner, W. Zettlemeyer, Handbook of Enantioselective Catalysis with Transition Metal Compounds, VCH, Weinheim, 1993.
[2] R.A. Sheldon, Chyrotechnology, Marcel Dekker, New York, 1993.
[3] R. Noyori, Asymmetric Catalysis in Organic Synthesis, Wiley–VCH, New York, 1994.
[4] C. Bolm, Chem. Rev. 103 (2003) 2361.
[5] A. Berkessel, H. Gröger, Asymmetric Organocatalysis, Wiley–VCH, Weinheim, 2005.
[6] Y. Orito, S. Imai, S. Niwa, J. Chem. Soc. Jpn. (1979) 1118.
[7] Y. Orito, S. Imai, S. Niwa, N.G. Hung, J. Synth. Org. Chem. 37 (1979) 173.
[8] B. Török, K. Felföldi, G. Szakonyi, K. Balázsik, M. Bartók, Catal. Lett. 52 (1998) 81.
[9] M. Sutyinszki, K. Szöri, K. Felföldi, M. Bartók, Catal. Commun. 3 (2002) 125.
[10] K. Balázsik, K. Szöri, K. Felföldi, B. Török, M. Bartók, Chem. Commun. (2000) 555.
[11] M. Studer, S. Burkhardt, H.U. Blaser, Chem. Commun. (1999) 1727.
[12] M. Studer, H.U. Blaser, C. Exner, Adv. Synth. Catal. 345 (2003) 45.
[13] T. Burgi, A. Baiker, Acc. Chem. Res. 37 (2004) 909.
[14] A. Baiker, Catal. Today 100 (2005) 159.
[15] D.Y. Murzin, P. Maki-Arvela, E. Toukoniitty, T. Salmi, Catal. Rev. Sci. Eng. 47 (2005) 175.
[16] G.J. Hutchings, Annu. Rev. Mater. Res. 35 (2005) 143.
[17] M. Bartók, Curr. Org. Chem. 10 (2006) 1533.
[18] O. Schwalm, B. Minder, J. Weber, A. Baiker, Catal. Lett. 23 (1994) 271.
[19] K.E. Simons, P.A. Meheux, S.P. Griffiths, I.M. Sutherland, P. Johnston, P.B. Wells, A.F. Carley, M.K. Rajumon, M.W. Roberts, A. Ibbotson, Recl. Trav. Chim. Pays-Bas 113 (1994) 465.
[20] A. Baiker, J. Mol. Catal. A Chem. 115 (1997) 473.
[21] R.L. Augustine, S.K. Tanielyan, J. Mol. Catal. A Chem. 112 (1996) 93.
[22] J.L. Margitfalvi, M. Hegedűs, J. Mol. Catal. A Chem. 107 (1996) 281.

[23] M. Bartók, M. Sutyinszki, K. Felföldi, Gy. Szöllősi, Chem. Commun. (2002) 1130.
[24] G. Vayner, K.N. Houk, Y.-K. Sun, J. Am. Chem. Soc. 126 (2004) 199.
[25] R.L. Augustine, S.K. Tanielyan, L.K. Doyle, Tetrahedron: Asymmetry 4 (1993) 1803.
[26] M. Bartók, K. Balázsik, F. Notheisz, React. Kinet. Catal. Lett. 77 (2002) 363.
[27] M. Bartók, K. Balázsik, T. Bartók, Z. Kele, Catal. Lett. 87 (2003) 235.
[28] S. Lavoie, P.H. McBreen, J. Phys. Chem. B 109 (2005) 11986.
[29] S. Lavoie, M.A. Laliberte, I. Temprano, P.H. McBreen, J. Am. Chem. Soc. 128 (2006) 7588.
[30] M. Bartók, K. Balázsik, I. Bucsi, Gy. Szöllősi, J. Catal. 239 (2006) 74.
[31] M. Bartók, P.T. Szabó, T. Bartók, Gy. Szöllősi, Rapid Commun. Mass Spectrom. 14 (2000) 509.
[32] N. Bonalumi, T. Bürgi, A. Baiker, J. Am. Chem. Soc. 125 (2003) 13342.
[33] M.S. Schneider, A. Urakawa, J.-D. Grunwaldt, T. Bürgi, A. Baiker, Chem. Commun. (2004) 744.
[34] S. Lavoie, M.-A. Laliberte, P.H. McBreen, J. Am. Chem. Soc. 125 (2003) 15756.
[35] S. Lavoie, M.-A. Laliberte, P.H. McBreen, Catal. Lett. 97 (2004) 111.
[36] J.M. Bonello, F.J. Williams, R.M. Lambert, J. Am. Chem. Soc. 125 (2003) 2723.
[37] E. Orglmeister, T. Mallat, A. Baiker, J. Catal. 234 (2005) 242.
[38] G.D.H. Dijkstra, R.M. Kellogg, H. Wynberg, J.S. Svendsen, I. Mako, K.B. Sharpless, J. Am. Chem. Soc. 111 (1989) 8069.
[39] G. Bond, P.B. Wells, J. Catal. 150 (1994) 329.
[40] J. Thiel, P. Fiedorow, J. Mol. Struct. 405 (1997) 219.
[41] W. Braje, J. Frackenpohl, P. Langer, H.M.R. Hoffmann, Tetrahedron 54 (1998) 3495.
[42] T. Bürgi, A. Baiker, J. Am. Chem. Soc. 120 (1998) 12920.
[43] D. Ferri, T. Bürgi, A. Baiker, J. Chem. Soc. Perkin Trans. 2 (1999) 1305.
[44] M. Maris, T. Bürgi, T. Mallat, A. Baiker, J. Catal. 226 (2004) 393.
[45] A. Vargas, T. Bürgi, A. Baiker, J. Catal. 222 (2004) 439.
[46] E. Toukoniitty, V. Nieminen, A. Taskinen, J. Paivarinta, M. Hotokka, D.Y. Murzin, J. Catal. 224 (2004) 326.
[47] A. Vargas, T. Bürgi, A. Baiker, J. Catal. 226 (2004) 69.
[48] N. Bonalumi, A. Vargas, D. Ferri, T. Burgi, T. Mallat, A. Baiker, J. Am. Chem. Soc. 127 (2005) 8467.
[49] R.T. Downs, R.M. Hazen, J. Mol. Catal. A Chem. 216 (2004) 273.
[50] A. Taskinen, E. Toukoniitty, Catal. Today 100 (2005) 373.
[51] J.W.D. Carneiro, C.D.B. de Oliveira, F.B. Passos, D.A.G. Aranda, P.R.N. de Souza, O.A.C. Antunes, J. Mol. Catal. A Chem. 226 (2005) 221.
[52] E.L. Jeffery, R.K. Mann, G.J. Hutchings, S.H. Taylor, D.J. Willock, Catal. Today 105 (2005) 85.
[53] J.W.D. Carneiro, C.D.B. de Oliveira, F.B. Passos, D.A.G. Aranda, P. Rogerio, P.R.N. de Souza, O.A.C. Antunes, Catal. Today 107–108 (2005) 31.
[54] V. Nieminen, A. Taskinen, E. Toukoniitty, M. Hotokka, D.Y. Murzin, J. Catal. 237 (2006) 131.
[55] A. Vargas, A. Baiker, J. Catal. 239 (2006) 220.
[56] C. Exner, A. Pfaltz, M. Studer, H.U. Blaser, Adv. Synth. Catal. 345 (2003) 1253.
[57] M. Bartók, M. Sutyinszki, K. Felföldi, J. Catal. 220 (2003) 207.
[58] B. Antalek, Concepts Magn. Reson. 14 (2002) 225.
[59] T.A. Halgren, J. Comput. Chem. 20 (1999) 720.
[60] M.J. Frisch, G.W. Trucks, H.B. Schlegel, G.E. Scuseria, M.A. Robb, J.R. Cheeseman, J.A. Montgomery Jr., T. Vreven, K.N. Kudin, J.C. Burant, J.M. Millam, S.S. Iyengar, J. Tomasi, V. Barone, B. Mennucci, M. Cossi, G. Scalmani, N. Rega, G.A. Petersson, H. Nakatsuji, M. Hada, M. Ehara, K. Toyota, R. Fukuda, J. Hasegawa, M. Ishida, T. Nakajima, Y. Honda, O. Kitao, H. Nakai, M. Klene, X. Li, J.E. Knox, H.P. Hratchian, J.B. Cross, C. Adamo, J. Jaramillo, R. Gomperts, R.E. Stratmann, O. Yazyev, A.J. Austin, R. Cammi, C. Pomelli, J.W. Ochterski, P.Y. Ayala, K. Morokuma, G.A. Voth, P. Salvador, J.J. Dannenberg, V.G. Zakrzewski, S. Dapprich, A.D. Daniels, M.C. Strain, O. Farkas, D.K. Malick, A.D. Rabuck, K. Raghavachari, J.B. Foresman, J.V. Ortiz, Q. Cui, A.G. Baboul, S. Clifford, J. Cioslowski, B.B. Stefanov, G. Liu, A. Liashenko, P. Piskorz, I. Komaromi, R.L. Martin, D.J. Fox, T. Keith, M.A. Al-Laham, C.Y. Peng, A. Nanayakkara, M. Challacombe, P.M.W. Gill, B. Johnson, W. Chen, M.W. Wong, C. Gonzalez, J.A. Pople, Gaussian 03, Revision C.02, Gaussian, Inc., Wallingford, CT, 2004; http://www.gaussian.com.
[61] K. Wolinski, J.F. Hilton, P. Pulay, J. Am. Chem. Soc. 112 (1990) 8251.
[62] T.A. Martinek, T. Varga, K. Balázsik, Gy. Szöllősi, F. Fülöp, M. Bartók, in preparation.
[63] S. Berger, S. Braun, 200 and More NMR Experiments. A Practical Course, Wiley–VCH, Weinheim, 2004.
[64] S. Bhattacharyya, B. Bagchi, J. Chem. Phys. 106 (1997) 1757.
[65] L. Jiang, L. Lai, J. Biol. Chem. 277 (2002) 37732.
[66] G.R. Desiraju, T. Steiner, The Weak Hydrogen Bond, Oxford Univ. Press, New York, 1999.
[67] B. Brutschy, Chem. Rev. 100 (2000) 3891.
[68] E.A. Reed, L.A. Curtiss, F. Weinhold, Chem. Rev. 88 (1988) 899.
[69] I.C. Lee, R.I. Masel, J. Phys. Chem. B 106 (2002) 368.
[70] A. Vargas, D. Ferri, A. Baiker, J. Catal. 236 (2005) 1.
[71] M. Bartók, M. Sutyinszki, I. Bucsi, K. Felföldi, Gy. Szöllősi, F. Bartha, T. Bartók, J. Catal. 231 (2005) 33.
[72] K. Szőri, K. Balázsik, K. Felföldi, M. Bartók, J. Catal. 241 (2006) 149.